Clinical & Translational Immunology

Australian and New Zealand Society for Immunology Inc.

Clinical & Translational Immunology 2021; e1313. doi: 10.1002/cti2.1313
www.wileyonlinelibrary.com/journal/cti

ORIGINAL ARTICLE

Generation of plasma cells and CD27^{-}IgD^{-} B cells during hantavirus infection is associated with distinct pathological findings

Priscilla F Kerkman[1†], Andy Dernstedt[1†], Lalitha Tadala[2,3], Eva Mittler[4], Mirjam Dannborg[2,3], Christopher Sundling[5,6], Kimia T Maleki[7], Johanna Tauriainen[7], Anne Tuiskunen-Bäck[1], Julia Wigren Byström[1], Pauline Ocaya[1], Therese Thunberg[1], Rohit K Jangra[4], Gleyder Román-Sosa[8], Pablo Guardado-Calvo[8], Felix A Rey[8], Jonas Klingström[7], Kartik Chandran[4], Andrea Puhar[2,3‡], Clas Ahlm[1‡] & Mattias NE Forsell[1]

[1]Department of Clinical Microbiology, Umeå Centre for Microbial Research (UCMR), Umea, Sweden
[2]The Laboratory for Molecular Infection Medicine Sweden (MIMS), Umeå Centre for Microbial Research (UCMR), Umea, Sweden
[3]Department of Molecular Biology, Umeå University, Umea, Sweden
[4]Department of Microbiology & Immunology, Albert Einstein College of Medicine, Bronx, NY, USA
[5]Department of Medicine, Karolinska Institutet, Solna, Sweden
[6]Department of Infectious Diseases, Karolinska University Hospital, Stockholm, Sweden
[7]Department of Medicine, Karolinska Institutet, Huddinge, Sweden
[8]Structural Virology Unit, Virology Department, Institut Pasteur, CNRS UMR 3569, Paris, France

Correspondence
MNE Forsell, Department of Clinical Microbiology, Section for Infection & Immunology, Umeå University, SE-901 87, Umea, Sweden.
E-mail: mattias.forsell@umu.se

†Equal contributors.
‡Equal contributors.

Received 28 May 2020;
Revised 19 April and 23 June 2021;
Accepted 23 June 2021

doi: 10.1002/cti2.1313

Clinical & Translational Immunology 2021; **10**: e1313

Abstract

Objective. Human hantavirus infections can cause haemorrhagic fever with renal syndrome (HFRS). The pathogenic mechanisms are not fully understood, nor if they affect the humoral immune system. The objective of this study was to investigate humoral immune responses to hantavirus infection and to correlate them to the typical features of HFRS: thrombocytopenia and transient kidney dysfunction. **Methods.** We performed a comprehensive characterisation of longitudinal antiviral B-cell responses of 26 hantavirus patients and combined this with paired clinical data. In addition, we measured extracellular adenosine triphosphate (ATP) and its breakdown products in circulation and performed *in vitro* stimulations to address its effect on B cells. **Results.** We found that thrombocytopenia was correlated to an elevated frequency of plasmablasts in circulation. In contrast, kidney dysfunction was indicative of an accumulation of CD27^{-}IgD^{-} B cells and CD27$^{-/low}$ plasmablasts. Finally, we provide evidence that high levels of extracellular ATP and matrix metalloproteinase 8 can contribute to shedding of CD27 during human hantavirus infection. **Conclusion.** Our findings demonstrate that thrombocytopenia and kidney dysfunction associate with distinctly different effects on the humoral immune system. Moreover, hantavirus-infected individuals have significantly elevated levels of extracellular ATP in circulation.

Keywords: antibodies, atypical B cells, B cells, haemorrhagic fever with renal syndrome, hantavirus, plasmablasts

INTRODUCTION

Hantaviruses can cause two major forms of human disease: hantavirus pulmonary syndrome (HPS) and haemorrhagic fever with renal syndrome (HFRS). Both of these diseases are characterised by endothelial cell dysfunction, vascular leakage and thrombocytopenia (reviewed in Hepojoki *et al*.[1]). Hantaviruses that cause HPS include the Andes and Sin Nombre strains in North and South America. During HPS, the hantavirus infection causes severe vascular leakage in the lung and up to 40% of patients die.[2] While lung pathogenesis has also been described for HFRS and the symptoms can be severe, strain-dependent mortality rates for HFRS can be as low as 0.4%.[2–4] Hantavirus strains that cause HFRS include the Hantaan, Dobrava, Seoul and Puumala (PUUV) strains. Of these, PUUV is present in several countries in Europe and endemic in the northern part including Scandinavia, Finland and Western Russia. To date, no efficacious treatment or vaccination regimen exists to protect against disease caused by hantavirus infections.

The well-controlled human studies have shown that hantavirus infections cause aberrant activation of both innate and adaptive immunity.[5–8] Furthermore, potent antiviral IgG-responses were associated with protection from severe disease during both HPS and HFRS,[9–12] and passive transfer of serum antibodies could reduce case fatality rate in a small cohort of HPS patients.[13] These findings clearly demonstrate that an activation of the humoral immune system and a subsequent elicitation of antiviral antibodies play a central role in the control of viremia and/or pathogenesis during hantavirus infections.

A recent study of HPS demonstrated levels of plasmablasts (PBs) and $CD27^{-}IgD^{-}$ B cells in circulation of patients.[14] The rapid and extensive PB response was similar in magnitude to what has been reported during acute dengue virus infection. This contrasts to the comparably moderate levels of PBs that are found in circulation during influenza infection or after influenza vaccination.[15] An expansion of the $CD27^{-}IgD^{-}$ B-cell subset has previously been shown for numerous inflammatory and infectious diseases, as well as during ageing and cancer.[16–21] However, it remains to be determined whether $CD27^{-}IgD^{-}$ B cells have a protective or detrimental role for humoral immune responses. The $CD27^{-}IgD^{-}$ B cells resemble memory B cells, have isotype switched and hypermutated B-cell receptors and likely originate from T cell-dependent germinal centre reactions in secondary lymphoid organs.[16,20] In systemic lupus erythematosus (SLE), an expanded population of $CD27^{-}IgD^{-}$ B cells was associated with the manifestation of nephritis in patients.[16] This suggests that the presence of $CD27^{-}IgD^{-}$ B cells may be linked to a reduced kidney function.

During HFRS-causing hantavirus infections, the reduced kidney function occurs independently of the severity of thrombocytopenia.[22,23] Detailed studies of humoral immune responses to hantavirus infections could therefore help to shed light on possible associations between antiviral B-cell response and the typical clinical features of HFRS, that is thrombocytopenia and kidney dysfunction. Here, we combined a comprehensive characterisation of antiviral B-cell responses with paired clinical data to better understand the effect of thrombocytopenia and kidney dysfunction for the development of antiviral humoral immunity.

We demonstrated that HFRS patients show unusually elevated levels of resting and activated PBs in circulation during the acute phase, and that this elevation correlated with the degree of thrombocytopenia. However, thrombocytopenia was not associated with a more potent antiviral antibody response. Instead, we showed that kidney dysfunction, as measured by serum creatinine during the acute-phase and the maximum levels reached throughout the disease, correlated with a relative longitudinal increase in antibody-mediated neutralisation of PUUV *in vitro*. Finally, we provide evidence that elevated levels of extracellular adenosine triphosphate (eATP) are present during hantavirus infection, which could drive matrix metalloprotease 8-mediated shedding of CD27 from human B cells. Collectively, we propose that eATP can, at least partially, explain the observed association between kidney dysfunction and increased numbers of $CD27^{-}IgD^{-}$ B cells in hantavirus patients.

RESULTS

Thrombocytopenia but not kidney dysfunction is associated with viremia during acute HFRS

To investigate B-cell dynamics during HFRS, we analysed peripheral blood mononuclear cells (PBMCs) and plasma/serum samples from 26 patients over time and 17 age- and sex-matched healthy controls. Age distribution and general characteristics of the cohorts are shown in Supplementary table 1. We collected and analysed longitudinal patient samples from acute (A) (days 5–9), intermediate (I) (days 10–21) and convalescent (C) (day > 34) phases of the disease (Figure 1a). At the time of inclusion, all patients had been diagnosed with acute PUUV infection by the detection of IgM against the virus nucleocapsid protein, and we subsequently determined acute virus load in plasma by PCR (Figure 1b). Consistent with previous studies, the disease manifested with an acute but transient reduction of circulating thrombocytes (Figure 1c) and elevated levels of serum creatinine and C-reactive protein (CRP) (Figure 1d and e). Viral load was only measured in acute sample as virus is rapidly cleared during HFRS.[9] In the acute phase, levels of thrombocytes inversely correlated with viral load ($r = -0.73$; $P < 0.0001$), but there was no significant correlation with the elevated levels of CRP and creatinine (Figure 1f). The lack of a correlation between thrombocytopenia and serum creatinine was in accordance with findings in a previous study of over 500 HFRS patients in Finland.[22] Collectively, these data suggested a potential use of longitudinal studies of HFRS to reveal whether thrombocytopenia or kidney dysfunction may differentially affect the humoral immune response to hantavirus infection.

Thrombocytopenia correlates with elevated levels of plasmablasts and plasma cells during HFRS

A transient elevation in the frequency of $CD19^+CD38^+CD20^-$ plasmablasts/plasma cells (PBs/PCs) in circulation was detected during the acute phase (gating strategy in Supplementary figure 1). Strikingly, several of the HFRS patients showed an extreme increase of PBs/PCs (comprising up to 80% of all circulating $CD19^+$ B cells) (Figure 2a). A similar extensive increase in PB had been reported to occur during HPS.[14] Phenotypical analysis revealed that HLA-$DR^{high}Ki67^+$ PB had reduced surface expression of HLA-DR during the acute phase (A vs. C: $P = 0.0013$; A vs. H $P < 0.0001$), whereas surface expression of CD38 was increased at the same time points (A vs. C: $P = 0.0047$; A vs. H: $P = 0.0024$) (Figure 2b). In addition, the frequency of $CCR10^+$ PBs was significantly increased during acute disease (A vs. C: $P = 0.0020$; A vs. H: $P = 0.032$) (Figure 2b). Since CCR10 expression is a common feature of IgA-producing PBs that originate from mucosal immune responses,[24,25] this is in line with PUUV infection triggering the development of IgA-producing PBs.[26] The fraction of PBs in patients that had upregulated CD138 in the acute phase was increased, as compared with the convalescent phase (Figure 2c). Consistent with the reduced HLA-DR on PBs, this demonstrated that hantavirus infection had led to an increased frequency of B cells undergoing terminal differentiation to PB and subsequently to mature PCs.[25,27] To better understand what drives the generation of PBs/PCs in circulation, we analysed whether the observed PB frequencies correlated with thrombocyte number and/or creatinine levels (Figure 2d). These analyses demonstrated a strong inverse correlation between thrombocyte numbers and both the frequency of PBs/PCs ($r = -0.74$; $P < 0.0001$) and expression of CD138 on PBs ($r = -0.50$; $P = 0.012$). As expected, we also found a strong correlation between the frequency of PBs/PCs and expression of the maturation marker CD138 on these cells during acute HFRS ($r = 0.64$; $P < 0.001$). Hence, both increased numbers and maturation status of PBs/PCs associated with the levels of thrombocytopenia but not with creatinine levels in the same patients.

Puumala virus infection can induce thrombocyte activation,[28] and both PUUV-induced HFRS and Andes virus-induced HPS can result in elevated levels of CXCL12. CXCL12 plays a role in PB/PC migration. To assess whether the infection may have mobilised resting PBs/PCs into circulation, we assessed the levels of proliferating PBs ($Ki67^+$) and non-proliferating ($Ki67^-$) PBs/PCs in circulation (Figure 2e). Consistent with an acute and antigen-driven B-cell response, the majority of PBs in circulation during acute HFRS were $Ki67^+$. However, the absolute numbers of $Ki67^-$ cells were also significantly elevated during the acute phase (Figure 2e). While we could not decipher whether this was a direct effect of

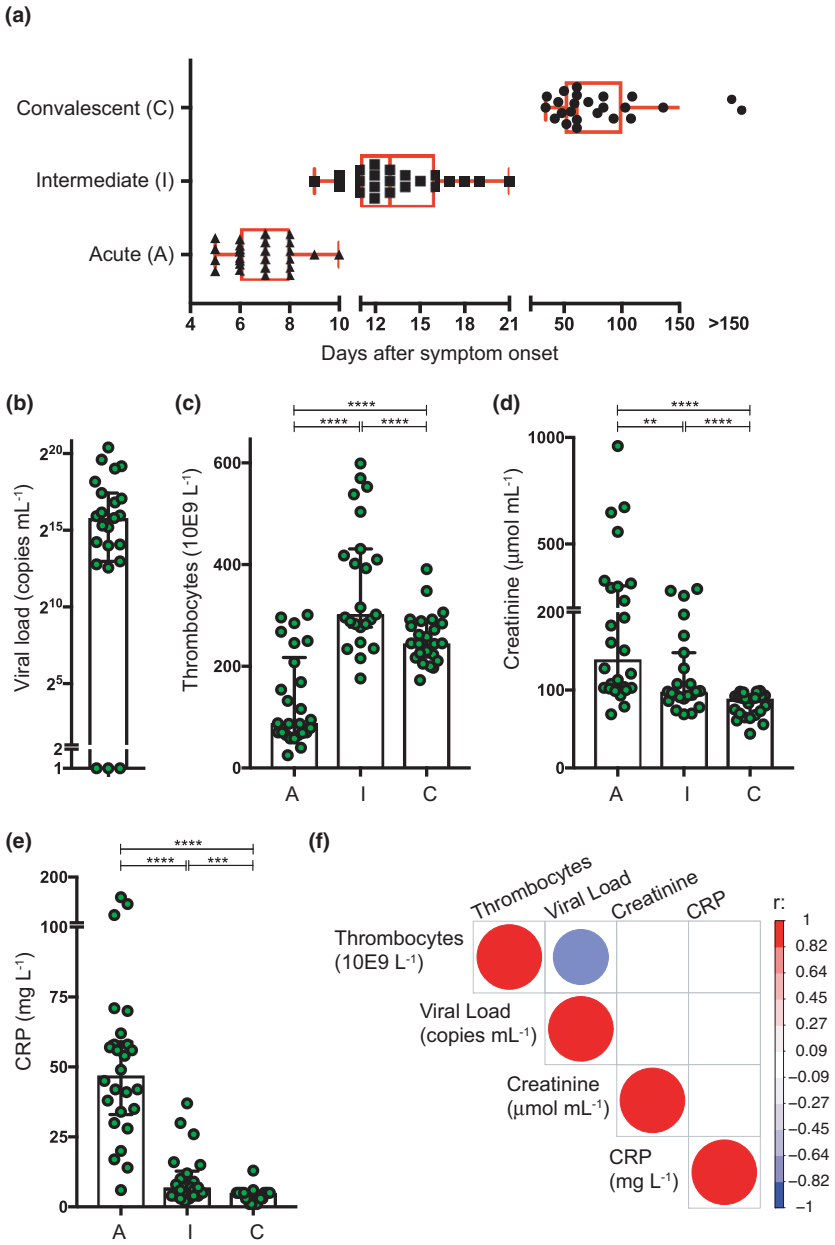

Figure 1. Viral load correlates with thrombocyte count but not with creatinine or CRP levels. **(a)** Schematic representation of time-points for collection of acute (*A*), intermediate (*I*) and convalescent (*C*) samples, based on time after disease onset. Because of availability of material for one donor, a day 9 sample was used as intermediate sample and for one donor a day 10 sample was used as acute sample. **(b)** Viral load at time of diagnosis. Viral load could not be detected in three patients that were diagnosed based on the presence of anti-PUUV IgM. For illustration purpose, these were set to 1. Thrombocyte count **(c)**, creatinine levels **(d)** and CRP **(e)** in plasma during acute, intermediate and convalescent phase of HFRS. **(f)** Correlative analysis of **(b–e)** were assessed according to non-Gaussian distributions using Spearman correlation. Correlations with *P*-values 0.05 or lower are shown. Thrombocytes (T) vs. Viral Load (VL): $r = -0.73$, $P < 0.0001$. T vs. Creatinine (Crea): $r = 0.11$, $P = 0.58$. T vs. CRP: $r = -0.38$, $P = 0.06$. VL vs. Crea: $r = -0.32$, $P = 0.14$. VL vs. CRP: $r = 0.13$, $P = 0.55$. Crea vs. CRP: $r = 0.14$ $P = 0.51$. Number of samples: $A = 26$; $I = 22$; $C = 24$.

thrombocytopenia, we found an increase in CXCL12 in circulation (median [IQR]: in acute phase 169 ng mL^{-1} [96-307 ng mL^{-1}] [$n = 25$]; convalescent 25 ng mL^{-1} [7–134 ng mL^{-1}] [$n = 13$]) that correlated with the frequency of PBs/PCs during acute HFRS [Figure 2f].

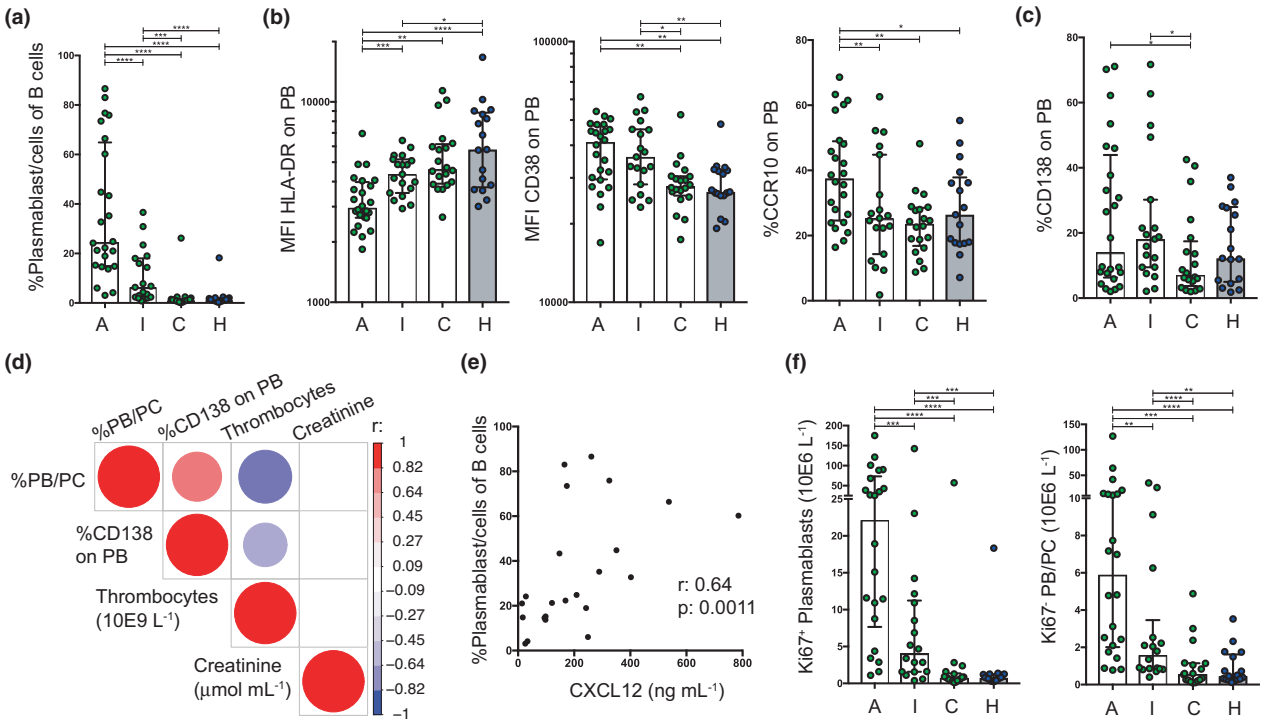

Figure 2. Frequency and absolute number of plasmablasts and plasma cells during infection correlates with thrombocyte count. **(a)** Frequency of PBs/PCs of total B cells during acute (*A*), intermediate (*I*) and convalescent (*C*) phase of disease in comparison with healthy controls (H). **(b)** Expression of HLA-DR, CD38 and frequency of CCR10, on PBs (defined as HLA-DR^{high}Ki67^{+}). **(c)** Frequency of CD138 expression on PBs during acute infection. **(d)** Spearman correlation between number of thrombocytes, creatinine level, frequency of PBs/PCs and frequency of CD138 expression on PBs during acute infection. Correlations with *P*-values 0.05 or lower are shown. Thrombocytes (T) vs. %PB/PC: $r = -0.74$, $P < 0.0001$. T vs. %CD138: $r = -0.50$, $P = 0.012$. Crea vs. %PB/PC: $r = -0.01$, $P = 0.95$. Crea vs. %CD138: $r = -0.23$, $P = 0.27$. **(e)** Number of PBs (HLA-DR^{high}Ki67^{+}) (left) and Ki67^{-} PBs/PCs (right) during *A*, *I* and *C* phase of HFRS and healthy controls (*H*). Number of samples: $A = 24$; $I = 19$; $C = 19$; $H = 17$. Significance was assessed using Wilcoxon matched-pairs signed rank test within each patient and using Mann–Whitney tests between different individuals. **(f)** Spearman correlation between level of CXCL12 in plasma and frequency of PBs/PCs during acute infection.

Thrombocytopenia is associated with decreased nucleocapsid-binding IgG during acute infection

To understand whether thrombocytopenia or kidney dysfunction could affect development of antiviral humoral immunity, we characterised the quantity and quality of antiviral antibodies in longitudinal plasma samples of patients with HFRS. We found that total circulating IgG, as well as albumin, was reduced during the acute phase of disease, but these values had normalised at the convalescent phase (Supplementary figure 2a). The reduction of albumin and IgG in circulation most likely reflected increased vascular and glomerular permeability that has been shown to increase clearance of albumin and IgG from the vascular to interstitial space and into urine.[29,30] Subsequently, we assessed binding properties of plasma antibodies to the highly expressed nucleocapsid (N) protein and to the viral spike protein Gn of PUUV and found that both N- and Gn-binding IgG had been elicited in all patients during acute HFRS and that the overall PUUV-binding potential had increased over time (N; $P = 0.0017$, Gn; $P = 0.045$) (Figure 3a). We found that the amount of N- and Gn-binding IgG between acute and convalescent phase of HFRS inversely correlated with thrombocyte numbers in patients ($r = -0.50$; $P = 0.016$ and $r = -0.45$; $P = 0.032$, respectively, Figure 3b). In contrast, patients where thrombocyte numbers had remained high during the acute phase of disease had N-binding IgG with increased binding capacity in circulation ($r = 0.54$; $P = 0.0076$, Figure 3b). Normalisation of N- and Gn-binding IgG with total IgG levels showed similar results, with a relative increase of N-binding IgG, and a

trend of increased Gn-binding IgG over time (Supplementary figure 2b). In patients with HPS, it was demonstrated that a similar extensive PB expansion leads to increased levels of autoantibodies in circulation.[14] Here, we could not find an association with anti-dsDNA or anti-Sjögrens syndrome-related antigen A, and while five patients had elevated anti-rheumatoid factor IgM antibodies, this did not correlate with the levels of PBs/PCs in circulation (Supplementary figure 2c). Collectively, these data demonstrated that, as expected, HFRS had induced accumulation and/or increased affinity of PUUV N- and Gn-specific IgG over time, but that vascular leakage during the acute phase of disease may impact on levels of virus-binding IgG in circulation. Of the two specificities we had measured, only antibodies directed to the envelope glycoprotein Gn can directly bind and neutralise functional PUUV particles. We therefore proceeded to assess whether the elicited antiviral antibodies could mediate neutralisation of virus infection, *in vitro*.

High creatinine levels are correlated with longitudinal qualitative development of neutralising antibodies

To assess the quality of the antiviral humoral immune response in patients, we determined the capacity of plasma antibodies to inhibit *in vitro* infection of target cells with 'wild-type' Kazan-strain PUUV. We found that potent neutralising antibodies were present in plasma from all patients at the time points tested. In this assay, 50% inhibition was reached at reciprocal plasma dilution between 10^3 and 10^5 (EC50, Figure 3c). This assay quantified total levels of virus RNA in infected cultures, and it was possible that our results had been affected by differential capacity of virus quasi-species to replicate in the target cells, as previously shown.[31] To reduce potential confounding factors, we subsequently assessed the capacity of plasma from HFRS patients to inhibit infection of target cells by a recombinant vesicular stomatitis virus that expressed the fluorophore mNeongreen and utilised the PUUV spike proteins Gn/Gc for attachment and entry into target cells (rVSV mNG-P PUUV Gn/Gc). This assay confirmed that neutralisation was directed against the viral spike proteins, and the 50% inhibitory activity was similar to inhibition of 'wild-type' virus infection (between 10^3 and 10^5, EC50, Figure 3d). Consistently, we also found a strong correlation between neutralisation and the level of Gn-binding ($r = 0.66$; $P = 0.0094$), but not N-binding antibodies (Figure 3e). Since thrombocytopenia correlated with a longitudinal increase in the binding capacity of plasma IgG to Gn, we assessed if the same was true for the neutralisation capacity of plasma from these patients. Here, the number of thrombocytes in patients did not correlate with neutralisation of rVSV mNG-P PUUV Gn/Gc at any time point, nor with the relative change in neutralisation capacity over time (Figure 3f). In contrast, we found a strong correlation between creatinine levels at the acute phase of disease and an increased capacity of plasma to neutralise VSV-bearing PUUV Gn/Gc over time, *in vitro* ($r = 0.59$; $P = 0.022$). The correlation was even stronger when the maximum creatinine level measured during the infection was assessed for each patient ($r = 0.74$; $P = 0.0022$). Hence, the two hallmark symptoms of HFRS, thrombocytopenia and kidney dysfunction, were differentially associated with the longitudinal development of binding and neutralising antibodies during HFRS.

HFRS patients with kidney dysfunction show increased frequency of $CD27^{low}$ plasmablasts and $CD27^{-}IgD^{-}$ B cells

During our investigations, we found that a number of HFRS patients had unusually low expression of CD27 of the surface on their PBs/PCs (Figure 4a). In contrast to the frequency of PBs/PCs in circulation, the expression levels of surface CD27 on PB/PCs did not correlate with thrombocyte numbers ($r = 0.074$; $P = 0.74$), but inversely correlated with serum creatinine levels in patients during acute disease ($r = -0.41$; $P = 0.05$, Figure 4b). Previously, it has been observed that isotype-switched B cells with low surface expression of CD27 ($CD27^{-}IgD^{-}$ B cells) accumulate in SLE patients with nephritis.[16] To further investigate the relationship between $CD27^{-}IgD^{-}$ B cells and kidney dysfunction during HFRS, we set out to characterise longitudinal changes in the circulating pool of B cells in patients. First, we determined that the absolute number of total B cells ($CD19^{+}$) did not significantly change over the acute, intermediate or convalescent phases (Figure 4c). We then focused on the frequency distribution within the $CD20^{+}$ B cells of naïve B cells ($CD27^{-}IgD^{+}$), unswitched memory B cells ($CD27^{+}IgD^{+}$), switched

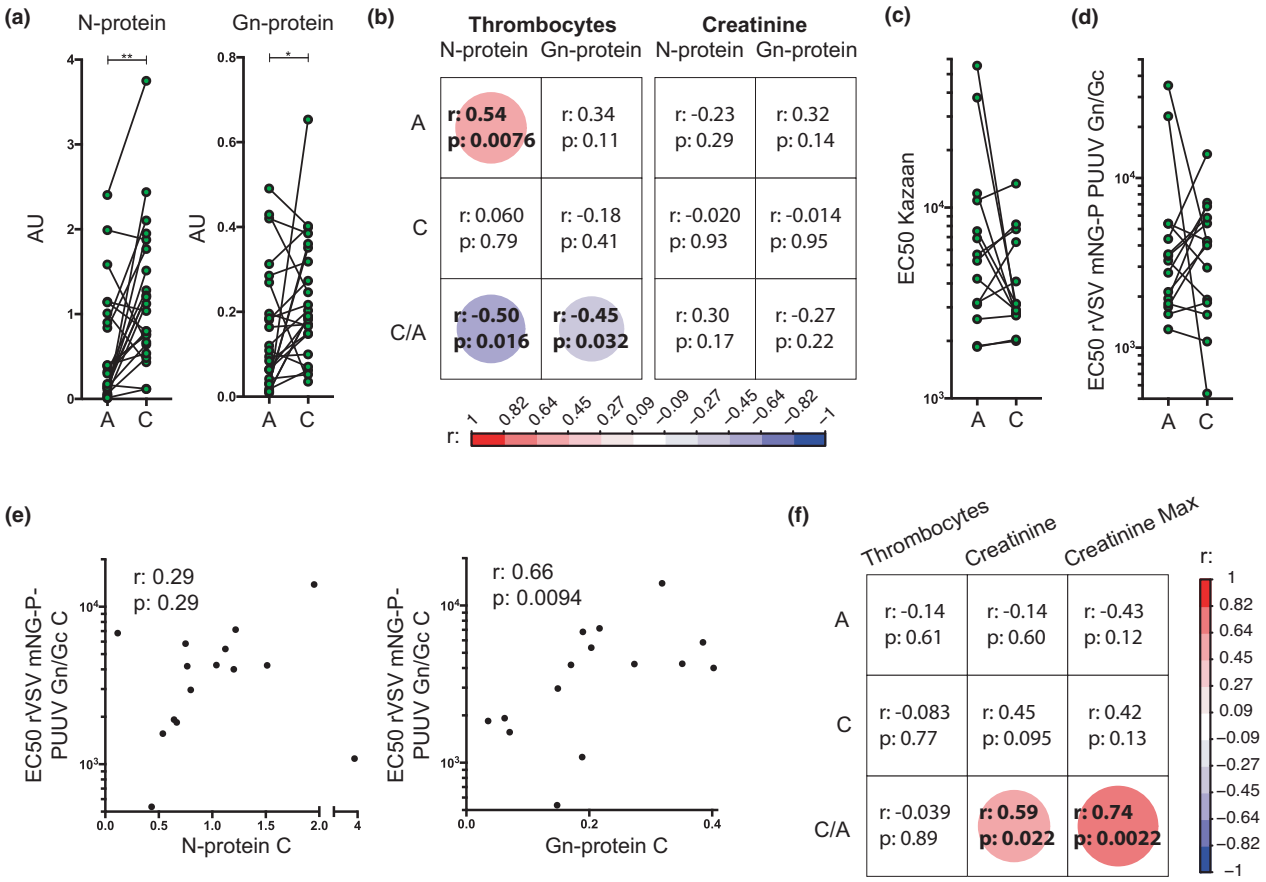

Figure 3. Creatinine levels correlate with the development of neutralising antibodies. **(a)** Quantification of N- and Gn-binding IgG in acute (*A*) and convalescent (*C*) plasma (n = 23) by ELISA. **(b)** Spearman correlation of thrombocyte number and creatinine level during acute infection with quantity during acute and convalescent phase (*A* & *C*) and increase (C/A) in PUUV N- and Gn-binding IgGs. **(c)** *In vitro* neutralisation of PUUV Kazan strain by patient plasma. Reciprocal plasma dilutions to achieve 50% neutralization are shown (EC50) (n = 14). **(d)** *In vitro* neutralisation of VSV mNG-P PUUV Gn/Gc by patient plasma. Reciprocal plasma dilutions to achieve 50% neutralisation are shown (n = 14). **(e)** Spearman correlation between quantity of PUUV N- and Gn-binding IgG and VSV mNG-P PUUV Gn/Gc neutralisation in convalescent plasma. **(f)** Spearman correlation of thrombocyte count and creatinine levels during acute infection and maximum creatinine with neutralisation capacity using the VSV mNG-P PUUV Gn/Gc readout during acute (*A*) and convalescent (*C*) phases and the ratio of neutralisation between convalescent and acute phase of HFRS (*C/A*).

memory B cells ($CD27^+IgD^-$) and double-negative B cells ($CD27^-IgD^-$) (complete gating strategy in Supplementary figure 1). The relative frequency of switched memory and naïve B cells remained similar over time, as compared with uninfected controls (Figure 4d). In contrast, the relative frequency of unswitched $CD27^+IgD^+$ memory B cells was significantly reduced during the acute and intermediate phases and the frequency of $CD27^-IgD^-$ B cells was significantly elevated throughout the disease (Figure 4d). The expression level of CD27 on PBs and the frequency of $CD27^+CD20^+$ B cells showed a positive correlation (r = 0.76; P < 0.001, Figure 4b). This suggested that the level of surface CD27 expression on PBs and B cells was linked. In contrast to PBs, we found only a trend between the frequency of B cells with low CD27 surface expression and creatinine levels (r = –0.37; P = 0.08). This suggested that creatinine did not directly affect CD27 expression and that there may be a factor present in tissues or circulation during HFRS that could separately affect creatinine, and CD27 expression levels on B cells. Increased creatinine levels[32] and accumulation of $CD27^-IgD^-$ B cells in circulation[18] have been reported to increase with age, but we could not find evidence that this had contributed to the

decreased expression of CD27 on B cells (Supplementary figure 3). We therefore proceeded to further characterise the CD27$^-$IgD$^-$ B-cell population that had accumulated in circulation during HFRS.

Circulating CD27$^-$IgD$^-$ B cells during HFRS comprise activated and resting B cells

Expression of intracellular Ki67 is increased during proliferation of cells,[33] and activated B cells increase expression of the transferrin receptor CD71 on their cell surface.[34] To better understand how CD27$^-$IgD$^-$ B cells had responded to PUUV infection, we investigated their dual expression of CD71 and Ki67 and compared this to classical switched CD27$^+$IgD$^-$ memory B cells during HFRS. We found that a median of 12.3% of the CD27$^-$IgD$^-$ B cells and 15.6% of CD27$^+$IgD$^-$ B cells were activated and proliferating during acute HFRS (Figure 5a, left panel). This difference between isotype-switched CD27$^-$ and CD27$^+$ B cells was significant throughout the acute, intermediate and convalescent phases of HFRS, and is consistent with a similar difference between the CD27$^-$IgD$^-$ and CD27$^+$IgD$^-$ B cells in healthy individuals (P(acute) = 0.0010; P(intermediate) < 0.0064; P(convalescent) < 0.0001; P(healthy) = 0.049) (Figure 5a, right panel). An increase in CD38 expression is indicative of an

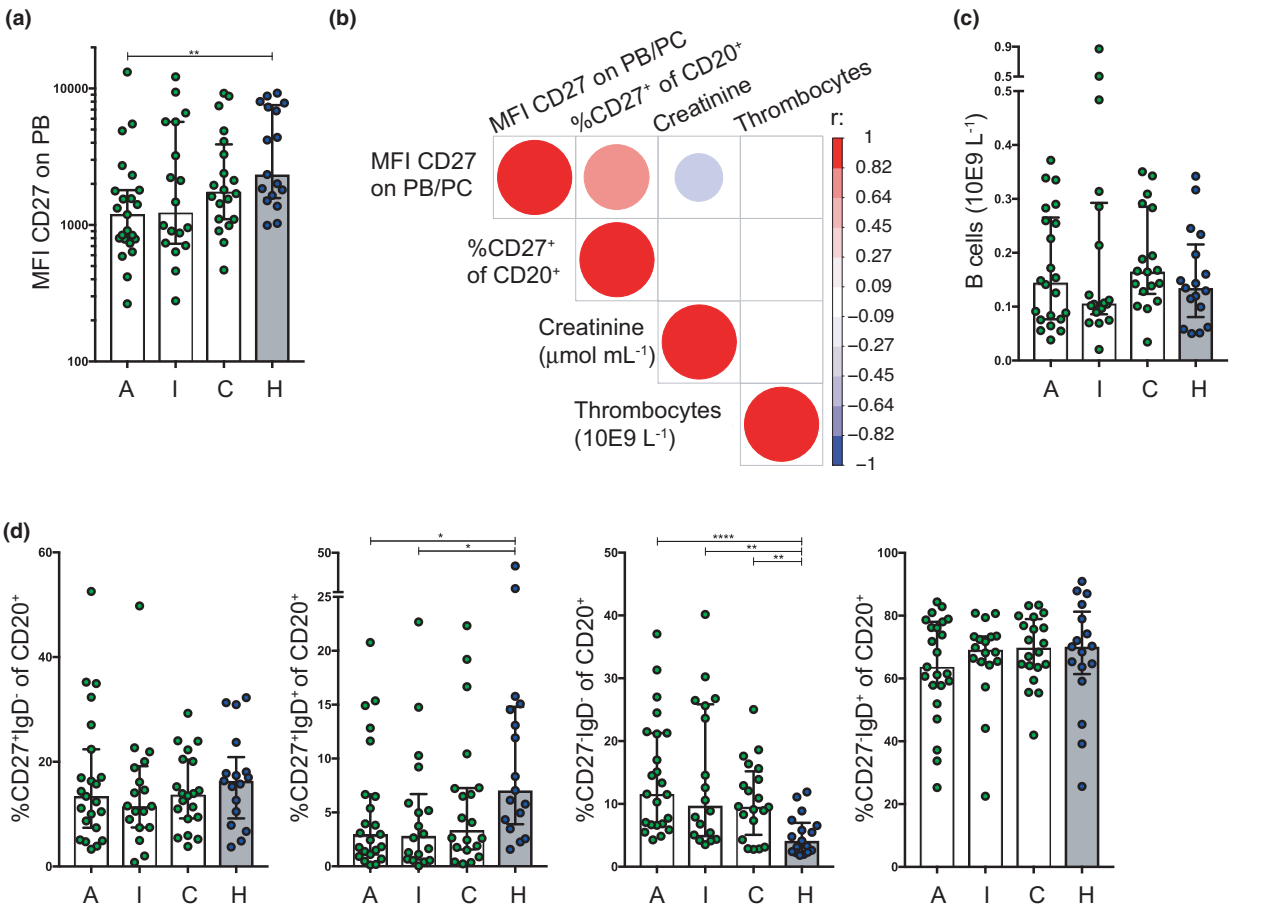

Figure 4. CD27 expression is decreased during acute HFRS infection, which correlates with increased creatinine levels. **(a)** Expression of CD27 on plasmablasts at different stages of disease, acute (*A*), intermediate (*I*) and convalescent (*C*) of HFRS and on healthy controls (*H*). **(b)** Spearman correlation between thrombocyte count, creatinine level, median CD27 expression on PB/PC and frequency of CD27 expressing CD20$^+$ B cells during acute infection. Correlations with *P*-value 0.05 or lower are shown. **(c)** Absolute number of B cells at different stages of disease and in healthy controls. **(d)** Frequencies of CD20$^+$ B-cell subpopulations at different stages of disease and in healthy controls. Number of samples: *A* = 24; *I* = 19; *C* = 19; *H* = 17. **(a), (c)** and **(d)** Significance was assessed using Wilcoxon matched-pairs signed rank test within each patient and using Mann–Whitney tests between different individuals.

active B-cell response, and a significant elevation of this marker was found on both $CD27^{-}IgD^{-}$ and $CD27^{+}IgD^{-}$ B cells (Figure 5b, left panel). Even though the HLA-DR expression on $CD27^{-}IgD^{-}$ and $CD27^{+}IgD^{-}$ B cells had remained unaltered throughout the infection (Figure 5b, right panel), both the ratios of CD38 and HLA-DR expression between the two subsets of isotype-switched B cells significantly decreased during acute infection compared to the convalescent phase (CD38; $P = 0.0016$, HLA-DR; $P = 0.004$) and to healthy controls (CD38; $P = 0.0015$, HLA-DR; $P = 0.0002$) (Supplementary figure 4). Thus, the $CD27^{-}IgD^{-}$ B cells showed reduced activation potential as compared with $CD27^{+}IgD^{-}$ B cells.

It was previously described that a subset of $CD27^{-}IgD^{-}$ B cells may comprise atypical B cells that are proposed to be exhausted during several chronic infectious or inflammatory diseases.[35,36] The expression of the inhibitory Fc receptor-like protein 5 (FcRL5) can be used to define atypical B cells within the $CD27^{-}IgD^{-}$ B-cell population,[37] and we proceeded to analyse $CD27^{-}IgD^{-}$ B cells during the acute phase of HFRS. We found that up to 60% of this B-cell subset were positive for FcRL5 expression (Figure 5c). Fcrl5 was also increased on the $CD27^{+}IgD^{-}$ population in patients, but this was lower than on the $CD27^{-}IgD^{-}$ population (not shown). To further verify that the $FcRL5^{+}$ cells in the $CD27^{-}IgD^{-}$ population were atypical B cells, we assessed whether $FcRL5^{+}$ or $FcRL5^{-}$ $CD27^{-}IgD^{-}$ B cells simultaneously expressed the integrin CD11c, the complement receptor 2 (CD21), the chemokine receptor CXCR3 and T-box transcription factor TBX21 (T-bet).[35,38,39] Consistent with an 'atypical' phenotype of $FcRL5^{+}$ cells, the frequency of CD11c, CXCR3 and T-bet were increased, whereas the frequency of CD21 expression was decreased in comparison with cells that were $FcRL5^{-}$ (Figure 5d). We also found an increased frequency of Ki67 expression in $FcRL5^{+}$ $CD27^{-}IgD^{-}$ B cells (Figure 5e). Thus, a large fraction of the atypical B cells had recently been proliferating, likely as a response to the hantavirus infection. In addition, these cells had increased expression of MHC class II (HLA-DR) in comparison with $FcRL5^{-}$ $CD27^{-}IgD^{-}$ B cells (Figure 5f). Since it was shown that atypical B cells downregulate transcription of CD27,[40] we assessed whether this was true also for the whole $CD27^{-}IgD^{-}$ B-cell population. Although we found that transcriptional downregulation of CD27 had occurred in the heterogeneous population of $CD27^{-}IgD^{-}$ B cells in both healthy controls and HFRS patients, the mRNA levels were generally higher than for naive $CD27^{-}IgD^{+}$ B cells in the same individuals (Figure 5g). This suggested that CD27 might be downregulated by an additional mechanism at the post-transcriptional level.

Elevated levels of ATP in circulation of HFRS patients

We first assessed whether altered CD27 expression could be induced by direct exposure of B cells to virus *in vitro* and found that neither short- or long-term exposure of PBMCs to PUUV reduced CD27 expression on isotype-switched IgD^{-} B cells (Figure 6a) (virus vs. ctrl: 2 h: $P = 0.69$; virus 2 h vs. 4 days: $P = 0.16$). However, we found elevated levels of soluble CD27 (sCD27) in circulation during the acute phase of HFRS, which correlated with high serum creatinine levels at the same time point ($r = 0.58$; $P = 0.0041$) (Figure 6b). This suggested that that shedding of CD27 from cells may be directly or indirectly linked to kidney dysfunction during HFRS. We therefore turned our attention to extracellular ATP (eATP), which had been implicated in regulation of kidney function[41] and shown to induce shedding of CD27 from mouse lymphocytes.[42] Elevated levels of eATP have been identified as part of the innate and adaptive immune response to viral infections[43–45] and also contribute to vaccine-induced responses by the oil-in-water squalene based adjuvant MF59.[46] We found that the average concentration of eATP in fresh plasma from 22 healthy individuals was 1.60 ± 0.58 μM. With this as baseline, we demonstrated that HFRS patients had elevated levels of eATP in plasma throughout the infection, including the convalescent phase (Figure 6c). As expected from the extremely short half-life of eATP and decay because of freeze thawing, we could not reliably detect ATP in frozen plasma samples. However, we could assess levels of the ATP breakdown-products adenosine, inosine and uric acid, and use these as an indicator for prior presence of extracellular ATP in frozen plasma samples from the 26 patients that this study was primarily based on.[45] To correct for differences in baseline between patients, we calculated a ratio based on the sum of breakdown products in plasma during acute infection divided by the sum of breakdown products in the paired convalescent plasma sample. By this, we found a correlation between

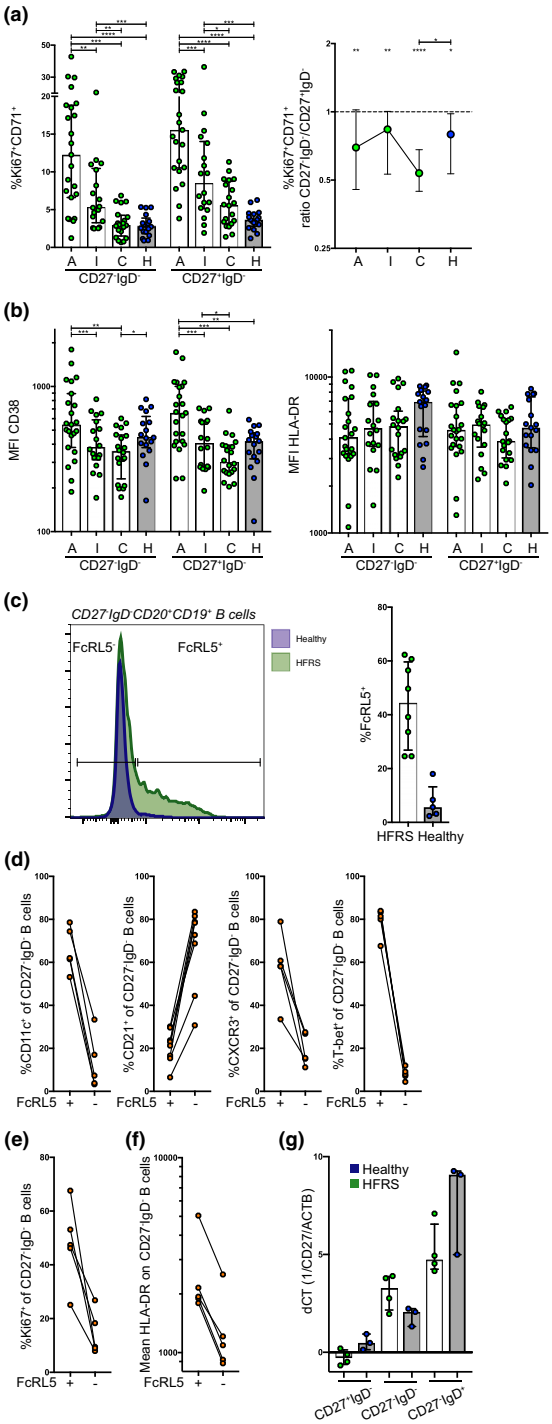

Figure 5. CD27$^-$IgD$^-$ B cells during HFRS have an increased frequency of atypical B cells. **(a)** Frequency of Ki67$^+$CD71$^+$ cells in CD27$^-$IgD$^-$ and CD27$^+$IgD$^-$ CD20$^+$ B cells (left) and difference in frequency within each individual (ratio: right panel). **(b)** Expression of CD38 and HLA-DR on CD27$^-$IgD$^-$ and CD27$^+$IgD$^-$ CD20$^+$ B cells. Plasma from acute phase (*A*): $n = 24$. Intermediate phase (*I*): $n = 19$. Convalescent phase (*C*) of disease: $n = 19$. Healthy (*H*) $n = 17$. Significance was assessed using Wilcoxon matched-pairs signed rank test within each patient and using Mann–Whitney tests between different individuals. **(c)** Left: representative histogram overlay of FcRL5 expression on CD27$^-$IgD$^-$ B cells. Right: frequency of FcRL5$^+$ CD27$^-$IgD$^-$ B cells during acute infection ($n = 8$) and healthy donors ($n = 4$). **(d)** Frequency of CD11c$^+$, CD21$^+$, CXCR3$^+$ and T-bet$^+$ of FcRL5$^+$ or FcRL5$^-$ CD27$^-$IgD$^-$ B cells. **(e)** Frequency of Ki67$^+$ expression on FcRL5$^+$ or FcRL5$^-$ CD27$^-$IgD$^-$ B cells. **(f)** Expression of HLA-DR on FcRL5$^+$ or FcRL5$^-$ CD27$^-$IgD$^-$ B cells. **(g)** RT-qPCR analysis of CD27 expression relative to beta-actin (*ACTB*) in CD27$^+$IgD$^-$, CD27$^-$IgD$^-$ and CD27$^-$IgD$^+$ B cells during acute infection and healthy donors (HFRS patients $n = 4$; healthy controls $n = 3$).

acute creatinine levels and the corrected levels of ATP breakdown products in the same patients ($r = 0.47$; $P = 0.024$, Figure 6d).

ATP- and MMP-8 mediated regulation of CD27 on human B cells *in vitro*

High levels of ATP have previously been shown to have an effect on immune cells, *in vitro*.[47] By co-incubation of PBMCs with increasing levels of ATP, we could demonstrate a modest and concentration-dependent decrease of CD27 on isotype-switched human B cells ($P = 0.0391$, 0.0078, Figure 6e, Supplementary figure 5a). The ATP levels required to reduce CD27 on B cells was significantly higher than the levels we could measure in circulation of patients. This may be a reflection of rapid degradation of ATP by B cells *in vitro* (Supplementary figure 5b). In support of shedding, we found a modest increase of sCD27 in supernatants from 5 of 7 donors after *in vitro* co-culture with ATP (Supplementary figure 5c). The decreased expression of CD27 on B cells was not reversed by addition of the P2 purinergic receptor inhibitor suramin, whereas co-incubation with an inhibitor for the matrix metalloproteinase 8 increased CD27 expression in 8 out of 9 donors after ATP stimulation (Figure 6f). We also found that ATP reduced CD23 on B cells in an ATP-dependent manner (Figure 6g) and, similarly, that co-incubation with an MMP-8 inhibitor, but not suramin, could reverse the reduction (Figure 6h). Since MMP-8 previously has been linked to shedding of CD27,[48] we measured MMP-8 in circulation of HFRS patients and found levels to be increased during the acute infection (Figure 6g).

DISCUSSION

By a comprehensive study of longitudinal PBMC and plasma samples from HFRS patients in Sweden, we could demonstrate that the two hallmark symptoms of the hantavirus infection, thrombocytopenia and kidney dysfunction, were associated with altered quantity and quality of antiviral B-cell responses, and that infection-induced eATP could have influenced the distribution of B-cell subsets in circulation.

A massive PB expansion in circulation has previously been shown during HPS and dengue virus infection.[14,15] Our data reveal that this expansion may be linked to thrombocytopenia during HFRS, a common symptom also for other hantavirus infections and dengue virus infection. We show that the expansion is, at least partially, because of mobilisation of both activated and resting PBs/PCs into circulation. Our data do not fully rule out that polyclonal expansion of B cells may have occurred, as previously suggested.[21] CXCL12, released upon thrombocyte activation, could potentially explain the increase of resting PBs/PCs in circulation, as CXCL12 is a well-known migratory chemokine for PBs/PCs. Since thrombocytopenia in viral haemorrhagic fevers is associated with vascular leakage and diffusion of antibodies from circulation into tissues, the expanded and activated PB/PC population may also be a response to compensate for this loss. Furthermore, other cells could be a potential source of CXCL12. Thrombocytes secrete other molecules, for instance sCD40L, that could also influence the B cell response. So far, information on direct or indirect crosstalk between thrombocytes and the humoral immune system during infection is sparse[49] and additional studies are required to dissect how and why the observed expansion occurs during both dengue virus and hantavirus infections.

One goal of our study was to evaluate whether thrombocytopenia or kidney dysfunction could be related to the ability of patients to mount antiviral antibodies. All patients in our study had developed neutralising antibodies to the virus, which demonstrates that neither of the symptoms had majorly affected the patients' capacity to mount an efficient humoral immune response. However, we did observe a positive correlation between serum creatinine and a relative increase in neutralisation potential over time in patients. Since we could not attribute this to a 'lower' starting potential of neutralisation during the acute phase, we speculate that patients who manifest with kidney dysfunction may have a more prominent infection and long-term inflammation that drives adaptive immunity. The documented adjuvant effect of eATP[46] suggests that the elevated levels of eATP could have contributed to the induced anti-PUUV antibody response. In contrast, the thrombocytopenia was not linked to plasma neutralisation potential but rather to an increase in overall PUUV-binding titres of plasma antibodies. While we did not specifically investigate the atypical B-cell subset in this study, acute PUUV-induced HFRS leads to elevated levels of IFN-gamma in circulation.[50]

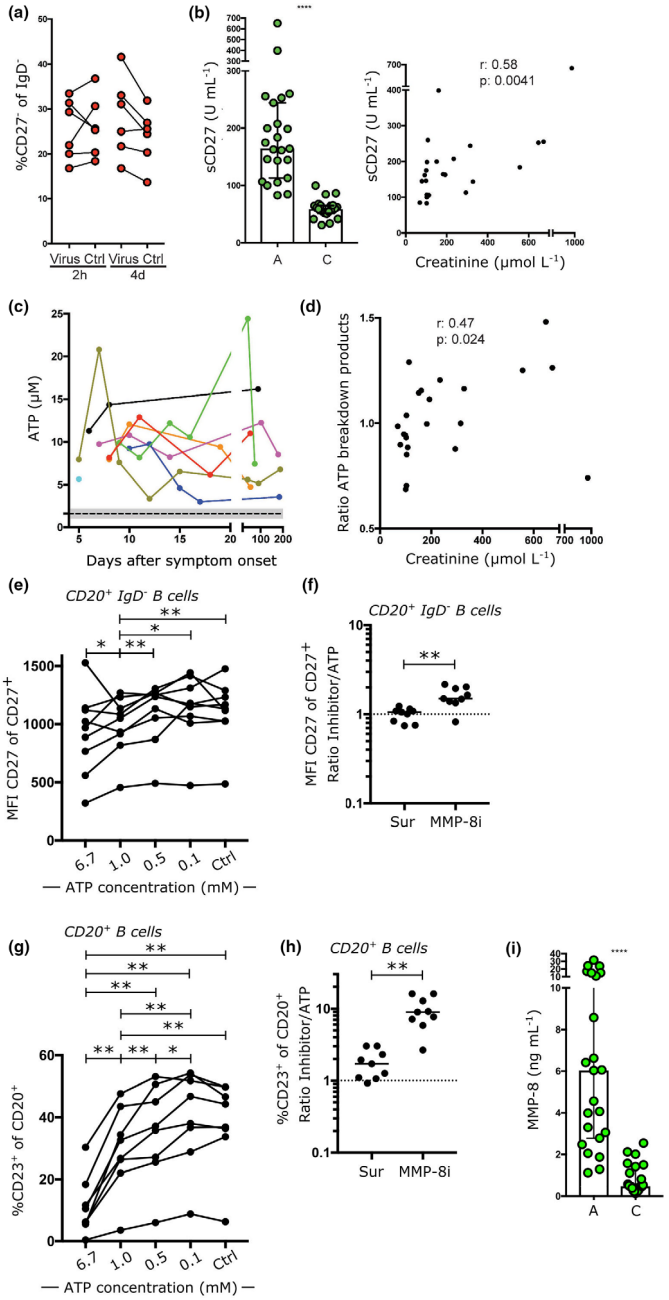

Figure 6. Extracellular ATP can induce shedding of CD27 from B cells. **(a)** Frequency of $CD27^{-}$ of IgD^{-} B cells or $CD23^{+}$ B cells 2 h and 4 d after exposure of PBMCs to PUUV (n = 6). Representative quantification from 3 independent experiments. **(b)** Quantification of sCD27 in patient plasma during acute and convalescent phase (left). Significance was assessed using Wilcoxon matched-pairs signed rank test within each patient. Spearman correlation between sCD27 and creatinine levels during acute infection is shown (right) (n = 23). **(c)** Measurement of ATP in fresh plasma at different time-points post onset of HFRS (n = 8). Black dotted line: average value measured in 22 healthy donors (11 males, 11 females); grey area standard deviation. **(d)** Spearman correlation between normalised ATP breakdown products in thawed plasma and creatinine levels form 23 donors with acute HFRS. **(e)** Quantification of CD27 expression on IgD^{-} B cells after incubation of PBMCs from 9 donors with increasing levels of ATP (one representative experiment of 4 is shown). **(f)** Relative increase in MFI of CD27 on IgD^{-} B cells after addition of suramin (*Sur*) or a MMP8 inhibitor (*MMP-8i*) to ATP-stimulated PBMCs. **(g)** Frequency of $CD23^{+}$ B cells after stimulation as in (**e**) (one representative experiment of 4 is shown). **(h)** Relative increase in frequency of $CD23^{+}$ on $CD20^{+}$ B cells after addition of suramin (*Sur*) or a MMP8 inhibitor (*MMP-8i*) to ATP stimulated PBMCs. **(i)** Quantity of MMP-8 in patient plasma during acute and convalescent phase (n = 23). Significance was assessed using Wilcoxon matched-pairs signed rank test within each patient **(e, i)**.

Therefore, the FcRL5$^+$ CD27$^-$IgD$^-$ atypical B-cell subset could have been generated by a similar B-cell receptor and IFN-gamma-dependent mechanism as was proposed for *Plasmodium falciparum* infection.[51] Collectively, we found no indication that CD27$^-$IgD$^-$ B cells, including the atypical B-cell subset, had negatively impacted the qualitative neutralising antibody response that was elicited upon PUUV infection. These data are in line with a recent study where the authors show that an elevation of CD27$^-$IgD$^-$ B cells in circulation was associated with increased immunity to infection with *Plasmodium falciparum*.[39]

An increased frequency of CD27$^-$IgD$^-$ B cells during kidney dysfunction in combination with a more severe disease and disease-specific autoantibodies had previously been described for SLE with nephritis.[16]

During our investigation, we unequivocally show that HFRS patients had elevated levels of eATP in circulation. eATP has previously been linked to kidney diseases,[41] viral infections[43–45] and shedding of CD27[42] and CD23.[52] One could speculate that the hantavirus infection or resulting sequelae[3,28] was the causative agent of the long-term elevation of eATP. An alternative explanation could be that individuals with intrinsically high eATP levels are more prone to have a clinical infection. Unfortunately, a lack of pre-HFRS samples from the patients prohibited us to investigate this further. We demonstrated that high levels of eATP could reduce CD27 levels on B cells *in vitro* and that an inhibitor for MMP-8 could reverse this. It should also be noted that the eATP concentration at the local site of release is significantly higher than what can be measured in circulation, where it is rapidly degraded.[53] Therefore, it is possible that CD27 cleavage occurs when B cells pass through inflamed and infected tissues rather than at all areas of the circulatory system. In this study, we could not determine if elevated MMP-8 levels during HFRS were a direct consequence of eATP during HFRS and a causative link remains to be investigated.

In summary, we here performed a comprehensive characterisation of kinetics and quality of B cell and antibody responses during PUUV infection. We demonstrate that neutralising antiviral antibodies and CD27$^-$IgD$^-$ B cells, including FcRL5$^+$ atypical B cells, in circulation accumulate in patients with kidney dysfunction during acute HFRS. Our findings also point towards eATP as a factor that can contribute to reduced CD27 on B cells and that may explain the association between CD27$^-$IgD$^-$ B cells and kidney dysfunction.[41] As a result of the role of eATP as mediator of systemic inflammation,[54] we propose that elevated levels of CD27$^-$IgD$^-$ B cells in circulation are, at least partially, a reflection of a vigorous strong immune reaction with no detriment for the development of efficient antiviral immunity. This is in line with recent findings that CD27$^-$IgD$^-$ B cells can be detected during normal immune reactions.[55] Our findings have implications for both our basic understanding of human B-cell responses to virus infections and reveal that ATP is released during acute hantavirus infection.

METHODS

Human subjects

Peripheral blood mononuclear cells (PBMC), plasma, serum and clinical parameters were collected from adult patients during Puumala virus (PUUV) infection longitudinally. PBMC and plasma from healthy individuals were also collected, stored and used as a control group. B cell and antibody characterisation were generated from samples from 26 PUUV-infected patients and 17 age- and sex-matched healthy volunteers except for data in Figure 4, in which samples from eight patients and four healthy donors were used. Additionally, fresh longitudinal plasma samples from eight patients monitored throughout the various stages of HFRS and 22 healthy controls were used for ATP measurements. Supplementary table 1 shows clinical characteristics of individuals studied.

Ethical statement

Ethical approval was obtained by the regional Ethical Review Board at Umeå University, Umeå, Sweden, Dnr. 04-113M and Dnr. 07-162M. Signed informed consent was obtained from all donors. No minors were included in this study. Infection and shedding experiments were performed on PBMC isolated from buffy coats obtained from the blood bank within the University hospital. No information was available on sex or age from these donors.

Quantification of viral load

RNA was prepared from 140 μL serum or plasma with QiaAmp Viral RNA Kit (Qiagen, Hilden, Germany) according to the manufacturer's instructions. Sixty microliter RNA was eluted. RNA (5 μL) was added to KAPA SYBR Fast Universal One-Step qRT-PCR Kit (15 μL) (KAPA Biosystems, Wilmington, MA, USA). Step One Plus Real Time PCR System (Applied Biosystems, Foster City, CA, USA) was used to perform the RT-qPCR. Analysis was performed with StepOne Plus Real-Time PCR System.

Flow cytometry

Peripheral blood mononuclear cells were thawed and subsequently surface stained with fixable aqua dead cell stain kit (Invitrogen, Carlsbad, CA, USA), CD24-BUV395 (clone ML5), CD138-BUV737 (clone MI15), CD3-AlexaFluor700 (clone UCHT1), CD14-AlexaFluor700 (clone M5E2), CD71-BrilliantViolet(BV)421 (clone M-A712), CD19-BV786 (clone SJ25C1), IL-6Ra-PE-CF594 (clone M5), IgG-PE-Cy5 (clone G18-145) (All BD Bioscience, Franklin Lakes, NJ, USA), BAFF-R-FITC (clone 11C1), CD20-APC (clone 2H7), CD16-AlexaFluor700 (clone 3G8), HLA-DR-APC-Cy7 (clone L243), IgD-BV605 (clone IA6-2), CD38-BV650 (clone HB-7) (all Biolegend, San Diego, CA, USA), CD27-biotin (clone O323, eBioscience, San Diego, CA, USA), Streptavidin-Qdot585 (Life Technologies, Carlsbad, CA, USA), CCR10-PE (clone 314305, R&D systems, Minneapolis, MN, USA) and IgA-PE-Vio770 (clone IS11-8E10, MiltenyiBiotec, Bergisch Gladbach, Germany). Cells were fixed and permeabilised with Foxp3/Transcription Factor Staining Buffer Set (eBioscience) and afterwards intracellularly stained with CD3-AlexaFluor700 and Ki-67-BV711 (clone Ki-67, Biolegend). In-depth analysis of $CD27^{-}IgD^{-}$ B-cell phenotype was performed with Fixable viability stain 780 or aqua viability dye V510, CD3-APC-Cy7 (clone SK7), CD14-APC-Cy7 (clone MΦP9), CD19-APC-R700, -PECy7 (clone HIB19), CD20-BB700 (clone 2H7), CD21-PE-Cy7, -BV421 (clone B-ly4), CD27-BV421, -BV786 (clone M-T271), IgD-BV510, -BB515 (clone IA6-2), CD95-PE-CF594 (clone DX2), CD38-PerCP-Cy5.5 (clone HIT2), CXCR3-PE-Cy5 (clone 1C6/CXCR3), HLA-DR-APC-H7 (clone G46-6), CD10-APC-R700 (clone HI10a), T-bet-AlexaFluor647 (clone4B10), CD11c-BV786 (clone B-ly6), CD39-BUV737 (clone TU66), Ki67-BUV395 (clone B56) (all BD Bioscience), FcRL5-PE (clone 509f6, Biolegend) and CD38-BV605 (clone HIT2) (Biolegend). To assess the effects of virus and ATP on B cells, PBMC was surface stained with CD3-APC-H7 (clone SK7), CD14-APC-H7 (clone HCD14), CD19-PE-CF594 (clone HIB19), CD20-AlexaFluor700 (clone 2H7), IgD-BV510 (clone IA6-2), CD23-PE (clone M-L233) and CD27-BV421 (clone M-T271) (all from BD Bioscience, except for CD20: Biolegend). Measurements were done on a BD Fortessa, LSRII and ARIAIII, and ZE5 Cell analyzer (Bio-Rad, Hercules, CA, USA), and subsequently analysed in DIVA (BD) or FlowJo.

Production and purification of recombinant Gn protein

In order to obtain soluble PUUV Gn, we inserted a synthetic gene codon-optimised for expression in Drosophila cells encoding amino acids 25–384 of Gn from the strain Sotkamo (NP_941983.1), into a modified pMT/BiP plasmid (Invitrogen) that encodes for a C-terminal strep-tag sequence. This plasmid was used to generate stable transfectants of Drosophila S2 cells together with the pCoPuro plasmid (ratio 1:20) for puromycin selection. The stable cell lines were selected and maintained in serum-free Insect-Xpress medium containing 7 μg mL^{-1} puromycin. Cultures of 1 L were grown in spinner flasks in Insect-Xpress medium supplemented with 1% penicillin/streptomycin antibiotics to about 1×10^7 cells mL^{-1}, and the protein expression was induced by adding 4 μM $CdCl_2$. After 5 days, the S2 media supernatant was concentrated to 40 mL and supplemented with 10 μg mL^{-1} avidin and 0.1 M Tris-HCl pH 8.0, centrifuged for 30 min at 20 000 *g* and purified by strep-tactin affinity chromatography and gel filtration. Fractions containing monomeric protein were pooled, concentrated in 10 mM Tris-HCl 8.0, 150 mM NaCl and frozen at −20°C.

Measurement of total and specific IgG

Total IgG in plasma was assessed using Human IgG ELISA Basic kit (Mabtech, Stockholm, Sweden) according to manufacturer's instructions. Antigen-specific antibody titres were assessed by coating 200 ng per well of either N protein or Gn protein on ELISA plates, and plasma samples were tested at dilutions 1:50, 1:500 and 1:5000. As standard, one patient plasma was chosen to be on all ELISA plates with a serial dilution starting at a 1:50 dilution. Quantity in figures is shown as arbitrary units (AU) where AU 1 is equal to the amount in the reference plasma. Detection and development were the same as the total IgG ELISA.

Expansion of PUUV Kazan and PBMC infection

Stocks of cell culture adapted PUUV Kazan strain were obtained by infecting confluent Vero E6 cells (ATCC, CRL1586, Manassas, VA, USA) in serum-free DMEM (Invitrogen) supplemented with Hepes (20 mM), $NaHCO_3$ (0.75 g L^{-1}), Penicillin-Streptomycin (10 000 U mL^{-1}) and pH 7.30 at 37°C shaking for 2 h. The viral inoculum was removed, and DMEM supplemented with 2% foetal bovine serum (FBS) (HyClone, Logan, UT, USA) was added to the cell cultures. After two virus expansion rounds of 7 days, supernatants were harvested and centrifuged at 433 *g*, 10 min, 4°C to remove debris, and ultracentrifuged through a sucrose coat in a SW 32 rotor in a Beckman Optima L-80 XP ultracentrifuge at 28 000 rpm at 4°C for 2 h. Virus pellets were suspended in serum-free DMEM supplemented as above and stored at –80°C. For infection experiments, PMBCs (200 000 cells per well) were seeded in a round-bottom, 96-well plate, and PUUV Kazan with MOI 100 in 30 μL was incubated for 2 h at 37°C with 5% CO_2. The inoculum was removed by aspiration, and cells were cultured in IMDM (Invitrogen) supplemented with 10% FBS (Gibco, Waltham, MA, USA) and penicillin-streptomycin for 96 h. Virus RNA was extracted from supernatant using NucleoSpin RNA kit (Macherey-Nagel, Bethlehem, PA, USA) and subsequently quantified using qPCR with KAPA Fast Universal one-step qRT-PCR kit (KAPA, Biosystems). Primers were provided by the Swedish Defense Research Agency with these sequences: Forward GAARTGGACCCGGATGACGTTAAC and reverse CKGGACACAGCATCTGCCATTC.

Cloning and rescue of rVSVs bearing PUUV Gn/Gc

Recombinant vesicular stomatitis Indiana viruses (rVSV) expressing an mNeongreen-phosphoprotein P fusion protein (mNG-P) has been described previously.[56] In this background, the VSV G gene was replaced with PUUV Gn/

Gc (strain CG1820/POR, GenBank accession number ALI59825.1) gene by using standard molecular biology techniques. rVSV-mNG-P-PUUV Gn/Gc viruses were generated by using a plasmid-based rescue system in 293T human embryonic kidney fibroblast cells (ATCC) (following published protocols).[56,57] Rescued virus was amplified on human hepatocarcinoma Huh.7.5.1 cells (a generous gift of Jan Carette, Stanford University, Stanford, CA, USA), and its identity was verified by sequencing of the Gn/Gc-encoding gene.

Neutralisation of wt PUUV and rVSVs bearing PUUV Gn/Gc

Vero E6 cells were seeded in a 96-well plate. The day after, plasma samples from patients were diluted in DMEM + 2% FBS + PUUV Kazan (MOI 8). Plasma and virus/DMEM solution were pre-incubated at 37°C 30 min. One hundred microliter plasma/virus/DMEM was added to each well and incubating at 37°C. At 20 h post-infection, cells were lysed and lysates were analysed by qRT-PCR with a Cells-to-CT Power SYBR Green kit (Invitrogen) according to the manufacturer's instructions. Two microliter of lysate was analysed per sample. The following PCR programme was used with StepOnePlus Real-Time PCR System (Applied Biosystems): 48°C 30 min, 95°C 10 min, (95°C 15 s, 60°C 1 min), 40 cycles. PCR results were used to determine plasma dilution needed to inhibit 50% of the maximum infection. For neutralisation assays, rVSV-mNG-P-PUUV Gn/Gc particles were incubated with 3-fold serial dilutions of human plasma at room temperature for 1 h, prior to addition to African grivet monkey kidney Vero cell (ATCC) monolayers in 96-well plates. Viral infectivity was measured by automated enumeration of mNG-positive cells using a CellInsight CX5 imager (Thermo Fisher, Waltham, MA, USA) at 12–14 h post-infection. After normalisation to no-plasma controls, the data were subjected to nonlinear regression analysis to determine plasma dilutions inhibiting 50% of infection and to extract half maximal effective concentration (EC_{50}) values (4-parameter, variable slope sigmoidal dose–response equation) using GraphPad Prism software (San Diego, CA, USA).

Quantification of CD27 mRNA

CD27 mRNA levels in different B-cell populations of PUUV patients were determined by sorting 500–1000 cells from each population. Sorting was done using a BD FACSAriaIII, and populations were defined as follows: switched memory $CD27^+IgD^-$, naïve: $CD27^-IgD^+$ and $CD27^-IgD^-$ cells; all pre-gated $CD3^-CD14^-CD19^+CD20^+$. Cells were sorted directly into lysis buffer from RNeasy Microkit (Qiagen). RNA was prepared according to manufacturer's instructions. RT-qPCR was performed in triplicates using the one-step system LightCycler 480 RNA Master Hydrolysis Probes (Roche, Basel, Switzerland), with the following PCR profile: 5 min 60°C, 1 min 95°C and (15 s 95°C, 1 min 60°C) 45 cycles, and run on a QuantStudio 5 machine. Commercially available primers from TaqMan were used to determine expression, and *CD27* expression was normalised to *ACTB*.

Measurement of sCD27, MMP-8 and CXCL12

Quantity of sCD27 was determined using sCD27 ELISA kit, and quantity of MMP-8 was determined using MMP-8 ELISA kit, both Invitrogen and used according to manufacturer's instructions. CXCL12 quantities were measured using human SDF-1 ELISA (BioSite, Mera Misa, CA, USA) kit according to manufacturer's instructions, with acute plasma samples diluted 1:100, and convalescent samples diluted 1:10.

Measurement of ATP, inosine and uric acid

ATP was quantified in fresh plasma only, as it does not resist freeze-thawing. A firefly luciferase-based sensitive ATP determination kit (Biaffin, Hessen, Germany) was used according to manufacturer's instructions. An ATP standard curve was freshly prepared in 50 mM phosphate buffer (1 M phosphate buffer stock: 0.477 mol KH_2PO_4 H_20; 0.523 mol $Na_2H_2PO_4$*$12H_20$; pH 7.4/NaOH; ad 1 L). Blood was collected in EDTA tubes, and the isolated plasma was diluted 1:50 in 50 mM phosphate buffer. As an additional control, spikes of known concentration of ATP (10 μM) were added to the diluted plasma samples to verify whether there were components in plasma that inhibit the assay reaction. Assay inhibition manifests as a quenched luminescence signal in spiked plasma with respect to spikes prepared in phosphate buffer and could hamper the quantification and the comparison of samples from different donors if not taken into account. The fraction of assay inhibition was calculated for every sample from the measured luminescence values using the formula: $L_{\text{spike in plasma}} - L_{\text{plasma}}/L_{\text{spike in buffer}}$. The obtained factor gives the fraction of the assay reaction that is not inhibited, where 1 means that there is no assay inhibition. All plasma samples showed comparable assay inhibition after dilution, that is from 0.8 to 1.2 for ATP.

A standard curve of inosine or uric acid was prepared in 50 mM phosphate buffer. We found that EDTA from collection tubes interfered with the assay. Therefore, an equal amount of $MgCl_2$ was added to the plasma. ATP breakdown products were measured in both diluted (1:100–1:800 in 50 mM phosphate buffer) and undiluted plasma samples. The assay was performed as described.[58] Spikes of known concentration of inosine (12.5 μM) or uric acid (25 μM) were added to the diluted plasma samples to verify whether there were components in plasma that inhibit the assay reaction. The fraction of assay inhibition was calculated for every sample from the measured fluorescence values using the formula: $F_{\text{spike in plasma}} - F_{\text{plasma}}/F_{\text{spike in buffer}}$. All plasma samples showed comparable assay inhibition after dilution, that is from 0.8 to 0.9 for inosine and 0.7 to 0.8 for uric acid.

The concentrations of ATP and ATP breakdown products in plasma samples were extrapolated from standard curves. Standard curves were constructed in Microsoft Office Excel.

CD27 shedding by ATP

Peripheral blood mononuclear cells from nine healthy donors were cultivated in RPMI-1640 without phenol red

and supplemented with 1% Penicillin-Streptomycin and 20 mM Hepes (all from Gibco), followed by incubation with ATP (Invitrogen, 6.7 mM), ATP and suramin (Sigma, St. Louis, MO, USA, 50 μM), ATP and MMP-8 inhibitor (Merck, 10 μM), Darmstadt, Germany) or control medium for 60 min at 37°C 5% CO_2. Subsequently, cells were analysed by flow cytometry on a ZE5 Cell Analyzer (Bio-Rad) for changes in surface expression and analysed as previously described with PCR for CD27 mRNA and supernatants were analysed for remaining ATP levels, and by ELISA for quantity of CD27. For assessing the capacity of B cells to break down ATP, B cells were isolated using EasySep Human B Cell Isolation Kit (StemCell Technologies, Vancouver, Canada), then cultivated and stimulated as described above. ATP concentrations in supernatants at multiple timepoints were measured, and CD27 expression on cells was assessed by flow cytometry.

Statistical analysis

Statistical analyses were performed using GraphPad Prism 7.0. To compare longitudinal differences within each donor, the significance was assessed using Wilcoxon matched-pairs signed rank tests. To compare material from different individuals, Mann–Whitney tests were used. Correlations were all assessed as non-Gaussian distributions using Spearman correlation. Bars represent the median with inter quartile range (IQR), with dots displaying all individual samples. *In vitro* shedding experiments were corrected for the control and afterwards assessed for significance using a Wilcoxon matched-pairs signed rank test, displayed as median with IQR. PCR results are displayed as mean (incl. standard deviation and all individual samples).

In general, each dot is data from one sample, ratio within one sample or ratio of longitudinal samples from one donor. sCD27 values from *in vitro* experiments: one dot is average sCD27 in culture wells from one donor. Significance was defined as follows: ns, $P > 0.05$; *, $P < 0.05$; **, $P < 0.01$; ***, $P < 0.001$; ****, $P < 0.0001$.

ACKNOWLEDGMENTS

This work was supported by the following grants: Intramural funds (AN 2.2.1.2-76-14) and Biotechnology grant (2.1.12-128714) from the Medical Faculty, Umeå University, and funds from the Swedish Society of Medicine (SLS-787091) to MF; research grants from the Västerbotten County Council (VLL-579011 and VLL-850681) to MF and CA; the Swedish Foundation for Strategic Research to CA and JK; the Knut and Alice Wallenberg Foundation (KAW 2015.0225) and Centre for Microbial Research (UCMR) and The Laboratory for Molecular Infection Medicine Sweden (MIMS) to AP; National Institutes of Health R01AI132633 to KC; the Swedish Science Council (2018-02646_3) and intramural funds from the Karolinska Institutet to JK.

CONFLICT OF INTEREST

The authors declare no conflict of interest.

AUTHOR CONTRIBUTION

Priscilla F Kerkman: Conceptualization, methodology, formal analysis, writing-original draft, writing-review and editing. **Andy Dernstedt:** Conceptualization, methodology, formal analysis, writing-review and editing. **Lalitha Tadala:** Methodology, formal analysis, writing-review and editing. **Eva Mittler:** Methodology, formal analysis, writing-review and editing. **Mirjam Dannborg:** Methodology, formal analysis, writing-review and editing. **Christopher Sundling:** Methodology, formal analysis, writing-review and editing. **Kimia T Maleki:** Methodology, writing-review and editing. **Johanna Tauriainen:** Methodology, writing-review and editing. **Anne Tuiskunen-Bäck:** Methodology, writing-review and editing. **Julia Wigren Byström:** Methodology, writing-review and editing. **Pauline Ocaya:** Methodology, writing-review and editing. **Therese Thunberg:** Resources, writing-review and editing. **RohitK Jangra:** Methodology, formal analysis, writing-review and editing. **Gleyder Román-Sosa:** Resources, writing-review and editing. **Pablo Guardado-Calvo:** Resources, writing-review and editing. **Felix A Rey:** Resources, writing-review and editing. **Jonas Klingström:** Formal analysis, writing-review and editing. **Kartik Chandran:** Formal analysis, writing-review and editing. **Andrea Puhar:** Conceptualisation, formal analysis, writing-review and editing. **Clas Ahlm:** Conceptualisation, formal analysis, writing-review and editing. **Mattias NE Forsell:** Conceptualization, formal analysis, writing-original draft, writing-review and editing.

REFERENCES

1. Hepojoki J, Vaheri A, Strandin T. The fundamental role of endothelial cells in hantavirus pathogenesis. *Front Microbiol* 2014; **5**: 727.
2. Vaheri A, Strandin T, Hepojoki J *et al*. Uncovering the mysteries of hantavirus infections. *Nat Rev Microbiol* 2013; **11**: 539–550.
3. Rasmuson J, Lindqvist P, Sorensen K, Hedstrom M, Blomberg A, Ahlm C. Cardiopulmonary involvement in Puumala hantavirus infection. *BMC Infect Dis* 2013; **13**: 501.
4. Hjertqvist M, Klein SL, Ahlm C, Klingstrom J. Mortality rate patterns for hemorrhagic fever with renal syndrome caused by Puumala virus. *Emerg Infect Dis* 2010; **16**: 1584–1586.
5. Bjorkstrom NK, Lindgren T, Stoltz M *et al*. Rapid expansion and long-term persistence of elevated NK cell numbers in humans infected with hantavirus. *J Exp Med* 2011; **208**: 13–21.
6. Lindgren T, Ahlm C, Mohamed N, Evander M, Ljunggren HG, Bjorkstrom NK. Longitudinal analysis of the human T cell response during acute hantavirus infection. *J Virol* 2011; **85**: 10252–10260.
7. Sane J, Laine O, Makela S *et al*. Complement activation in Puumala hantavirus infection correlates with disease severity. *Ann Med* 2012; **44**: 468–475.
8. Klingstrom J, Smed-Sorensen A, Maleki KT *et al*. Innate and adaptive immune responses against human Puumala virus infection: immunopathogenesis and suggestions for novel treatment strategies for severe hantavirus-associated syndromes. *J Intern Med* 2019; **285**: 510–523.

9. Pettersson L, Thunberg T, Rocklov J, Klingstrom J, Evander M, Ahlm C. Viral load and humoral immune response in association with disease severity in Puumala hantavirus-infected patients–implications for treatment. *Clin Microbiol Infect* 2014; **20**: 235–241.
10. Valdivieso F, Vial P, Ferres M *et al*. Neutralizing antibodies in survivors of Sin Nombre and Andes hantavirus infection. *Emerg Infect Dis* 2006; **12**: 166–168.
11. Evander M, Eriksson I, Pettersson L *et al*. Puumala hantavirus viremia diagnosed by real-time reverse transcriptase PCR using samples from patients with hemorrhagic fever and renal syndrome. *J Clin Microbiol* 2007; **45**: 2491–2497.
12. MacNeil A, Comer JA, Ksiazek TG, Rollin PE. Sin Nombre virus-specific immunoglobulin M and G kinetics in hantavirus pulmonary syndrome and the role played by serologic responses in predicting disease outcome. *J Infect Dis* 2010; **202**: 242–246.
13. Vial PA, Valdivieso F, Calvo M *et al*. A non-randomized multicentre trial of human immune plasma for treatment of hantavirus cardiopulmonary syndrome caused by Andes virus. *Antivir Ther* 2015; **20**: 377–386.
14. Garcia M, Iglesias A, Landoni VI *et al*. Massive plasmablast response elicited in the acute phase of Hantavirus Pulmonary Syndrome. *Immunology* 2017; **151**: 122–135.
15. Wrammert J, Onlamoon N, Akondy RS *et al*. Rapid and massive virus-specific plasmablast responses during acute dengue virus infection in humans. *J Virol* 2012; **86**: 2911–2918.
16. Wei C, Anolik J, Cappione A *et al*. A new population of cells lacking expression of CD27 represents a notable component of the B cell memory compartment in systemic lupus erythematosus. *J Immunol* 2007; **178**: 6624–6633.
17. Joosten SA, van Meijgaarden KE, Del Nonno F *et al*. Patients with tuberculosis have a dysfunctional circulating B-cell compartment, which normalizes following successful treatment. *PLoS Pathog* 2016; **12**: e1005687.
18. Colonna-Romano G, Bulati M, Aquino A *et al*. A double-negative ($IgD^{-}CD27^{-}$) B cell population is increased in the peripheral blood of elderly people. *Mech Ageing Dev* 2009; **130**: 681–690.
19. Centuori SM, Gomes CJ, Kim SS *et al*. Double-negative ($CD27^{-}IgD^{-}$) B cells are expanded in NSCLC and inversely correlate with affinity-matured B cell populations. *J Transl Med* 2018; **16**: 30.
20. Fecteau JF, Cote G, Neron S. A new memory $CD27^{-}IgG^{+}$ B cell population in peripheral blood expressing VH genes with low frequency of somatic mutation. *J Immunol* 2006; **177**: 3728–3736.
21. Yam-Puc JC, Cedillo-Barron L, Aguilar-Medina EM, Ramos-Payan R, Escobar-Gutierrez A, Flores-Romo L. The cellular bases of antibody responses during dengue virus infection. *Front Immunol* 2016; **7**: 218.
22. Outinen TK, Laine OK, Makela S *et al*. Thrombocytopenia associates with the severity of inflammation and variables reflecting capillary leakage in Puumala Hantavirus infection, an analysis of 546 Finnish patients. *Infect Dis* 2016; **48**: 682–687.
23. Mustonen J, Outinen T, Laine O, Porsti I, Vaheri A, Makela S. Kidney disease in Puumala hantavirus infection. *Infect Dis* 2017; **49**: 321–332.
24. Kunkel EJ, Kim CH, Lazarus NH *et al*. CCR10 expression is a common feature of circulating and mucosal epithelial tissue IgA Ab-secreting cells. *J Clin Invest* 2003; **111**: 1001–1010.
25. Mei HE, Yoshida T, Sime W *et al*. Blood-borne human plasma cells in steady state are derived from mucosal immune responses. *Blood* 2009; **113**: 2461–2469.
26. Björling E, de Carvalho Nicacio C, Lundkvist A. Immunoglobulin A responses to Puumala hantavirus. *J Gen Virol* 2000; **81**: 1453–1461.
27. Ellebedy AH, Jackson KJ, Kissick HT *et al*. Defining antigen-specific plasmablast and memory B cell subsets in human blood after viral infection or vaccination. *Nat Immunol* 2016; **17**: 1226–1234.
28. Connolly-Andersen AM, Sundberg E, Ahlm C *et al*. Increased thrombopoiesis and platelet activation in hantavirus-infected patients. *J Infect Dis* 2015; **212**: 1061–1069.
29. Ala-Houhala I, Koskinen M, Ahola T *et al*. Increased glomerular permeability in patients with nephropathia epidemica caused by Puumala hantavirus. *Nephrol Dial Transplant* 2002; **17**: 246–252.
30. Levitt DG, Levitt MD. Human serum albumin homeostasis: a new look at the roles of synthesis, catabolism, renal and gastrointestinal excretion, and the clinical value of serum albumin measurements. *Int J Gen Med* 2016; **9**: 229–255.
31. Sundstrom KB, Stoltz M, Lagerqvist N, Lundkvist A, Nemirov K, Klingstrom J. Characterization of two substrains of Puumala virus that show phenotypes that are different from each other and from the original strain. *J Virol* 2011; **85**: 1747–1756.
32. Tiao JY, Semmens JB, Masarei JR, Lawrence-Brown MM. The effect of age on serum creatinine levels in an aging population: relevance to vascular surgery. *Cardiovasc Surg* 2002; **10**: 445–451.
33. Scholzen T, Gerdes J. The Ki-67 protein: from the known and the unknown. *J Cell Physiol* 2000; **182**: 311–322.
34. Kehrl JH, Muraguchi A, Fauci AS. Differential expression of cell activation markers after stimulation of resting human B lymphocytes. *J Immunol* 1984; **132**: 2857–2861.
35. Karnell JL, Kumar V, Wang J, Wang S, Voynova E, Ettinger R. Role of $CD11c^{+}$ T-bet^{+} B cells in human health and disease. *Cell Immunol* 2017; **321**: 40–45.
36. Portugal S, Obeng-Adjei N, Moir S, Crompton PD, Pierce SK. Atypical memory B cells in human chronic infectious diseases: An interim report. *Cell Immunol* 2017; **321**: 18–25.
37. Sullivan RT, Kim CC, Fontana MF *et al*. FCRL5 delineates functionally impaired memory B cells associated with *Plasmodium falciparum* exposure. *PLoS Pathog* 2015; **11**: e1004894.
38. Sundling C, Ronnberg C, Yman V *et al*. B cell profiling in malaria reveals expansion and remodelling of $CD11c^{+}$ B cell subsets. *JCI Insight* 2019; **5**: e126492.
39. Sullivan RT, Ssewanyana I, Wamala S *et al*. B cell subtypes following acute malaria and associations with clinical immunity. *Malar J* 2016; **15**: 139.
40. Berggren O, Hagberg N, Alexsson A, Weber G, Ronnblom L, Eloranta ML. Plasmacytoid dendritic cells and RNA-containing immune complexes drive expansion of peripheral B cell subsets with an SLE-like phenotype. *PLoS One* 2017; **12**: e0183946.

41. Solini A, Usuelli V, Fiorina P. The dark side of extracellular ATP in kidney diseases. *J Am Soc Nephrol* 2015; **26**: 1007–1016.
42. Moon H, Na HY, Chong KH, Kim TJ. P2X7 receptor-dependent ATP-induced shedding of CD27 in mouse lymphocytes. *Immunol Lett* 2006; **102**: 98–105.
43. Zhang C, He H, Wang L *et al*. Virus-triggered ATP release limits viral replication through facilitating IFN-β production in a P2X7-dependent manner. *J Immunol* 2017; **199**: 1372–1381.
44. Seror C, Melki MT, Subra F *et al*. Extracellular ATP acts on P2Y2 purinergic receptors to facilitate HIV-1 infection. *J Exp Med* 2011; **208**: 1823–1834.
45. Bours MJ, Swennen EL, Di Virgilio F, Cronstein BN, Dagnelie PC. Adenosine 5′-triphosphate and adenosine as endogenous signaling molecules in immunity and inflammation. *Pharmacol Ther* 2006; **112**: 358–404.
46. Vono M, Taccone M, Caccin P *et al*. The adjuvant MF59 induces ATP release from muscle that potentiates response to vaccination. *Proc Natl Acad Sci USA* 2013; **110**: 21095–21100.
47. Mariathasan S, Weiss DS, Newton K *et al*. Cryopyrin activates the inflammasome in response to toxins and ATP. *Nature* 2006; **440**: 228–232.
48. Zhou Y, Liu X, Xu L *et al*. Matrix metalloproteinase-8 is overexpressed in Waldenstrom's macroglobulinemia cells, and specific inhibition of this metalloproteinase blocks release of soluble CD27. *Clin Lymphoma Myeloma Leuk* 2011; **11**: 172–175.
49. Assinger A. Platelets and infection - an emerging role of platelets in viral infection. *Front Immunol* 2014; **5**: 649.
50. Linderholm M, Ahlm C, Settergren B, Waage A, Tarnvik A. Elevated plasma levels of tumor necrosis factor (TNF)-α, soluble TNF receptors, interleukin (IL)-6, and IL-10 in patients with hemorrhagic fever with renal syndrome. *J Infect Dis* 1996; **173**: 38–43.
51. Obeng-Adjei N, Portugal S, Holla P *et al*. Malaria-induced interferon-γ drives the expansion of Tbet^{hi} atypical memory B cells. *PLoS Pathog* 2017; **13**: e1006576.
52. Gu B, Bendall LJ, Wiley JS. Adenosine triphosphate-induced shedding of CD23 and L-selectin (CD62L) from lymphocytes is mediated by the same receptor but different metalloproteases. *Blood* 1998; **92**: 946–951.
53. Di Virgilio F, Dal Ben D, Sarti AC, Giuliani AL, Falzoni S. The P2X7 Receptor in Infection and Inflammation. *Immunity* 2017; **47**: 15–31.
54. Cauwels A, Rogge E, Vandendriessche B, Shiva S, Brouckaert P. Extracellular ATP drives systemic inflammation, tissue damage and mortality. *Cell Death Dis* 2014; **5**: e1102.
55. Sutton HJ, Aye R, Idris AH *et al*. Atypical B cells are part of an alternative lineage of B cells that participates in responses to vaccination and infection in humans. *Cell Rep* 2021; **34**: 108684.
56. Kleinfelter LM, Jangra RK, Jae LT *et al*. Haploid genetic screen reveals a profound and direct dependence on cholesterol for hantavirus membrane fusion. *MBio* 2015; **6**: e00801.
57. Whelan SP, Ball LA, Barr JN, Wertz GT. Efficient recovery of infectious vesicular stomatitis virus entirely from cDNA clones. *Proc Natl Acad Sci USA* 1995; **92**: 8388–8392.
58. Puhar A, Tronchere H, Payrastre B, Nhieu GT, Sansonetti PJ. A Shigella effector dampens inflammation by regulating epithelial release of danger signal ATP through production of the lipid mediator PtdIns5P. *Immunity* 2013; **39**: 1121–1131.

Supporting Information

Additional supporting information may be found online in the Supporting Information section at the end of the article.